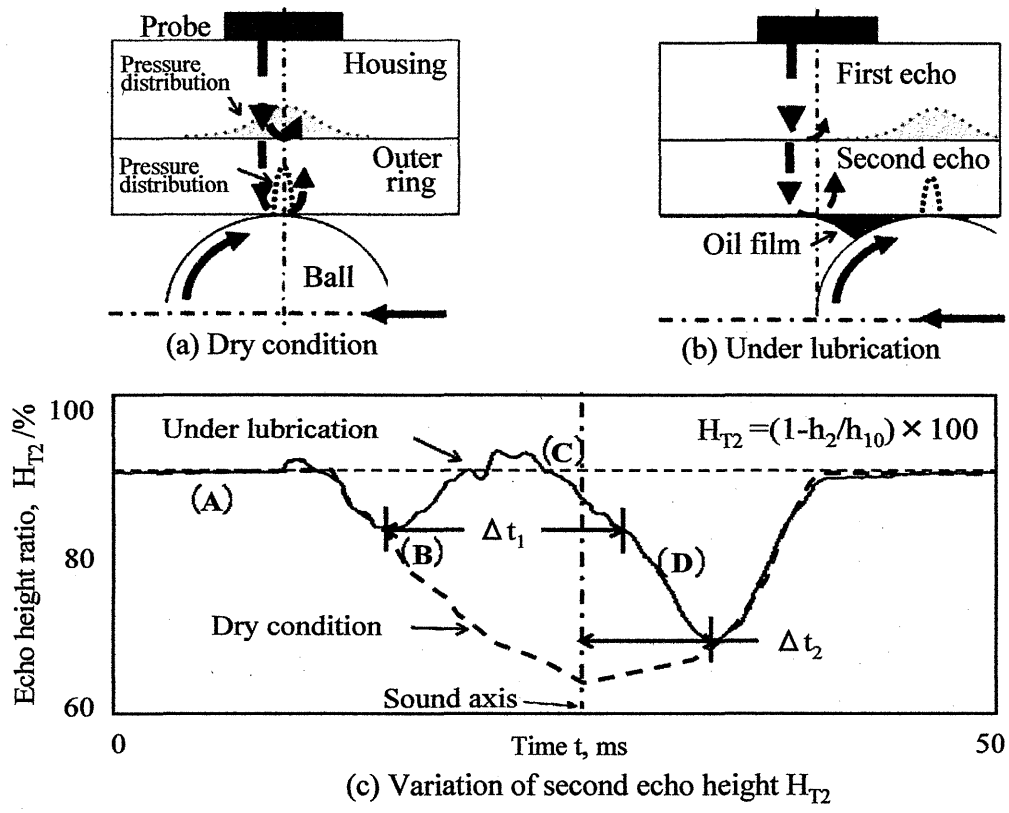

Figure 3 Evaluation indexes of oil supply condition

On the other hand, when sufficient oil is supplied to the inlet of contacting surface, the echo height that continued decrease as the ball approaches to the sound axis of ultrasonic probe is increased locally as shown by Δt_1 in Figure 3 (c) because ultrasonic wave is transmitted to the oil film. The oil film formation region at the inflow side to contribute for transmission of ultrasonic wave is wider than that of exit side, as shown in Figure 3 (b). Then, a peak of convex curve of H_{T2} appears at inflow side of the ball, and H_{T2} reduces up to dashed line which shows dry condition as the inflow side of ball goes away from the sound axis.

Therefore, it is possible to evaluate the condition of oil film formation at inflow side with degree of increment of H_{T2} there. However, the amplitude of H_{T2} is influenced with not only the oil film formation but also the contact condition between housing and outer ring. Since this contact condition varies during operation, h_0 from its interface and h_2 from the interface of outer ring and ball are varied with time, even if oil film formation is the same. Thus amplitude of H_{T2}, $(1-h_2/h_0)\times 100$, is unsuitable for the index of oil insufficiency.

Therefore, duration time Δt_1 that increment of H_{T2} is kept is employed as an index of insufficient oil supply, in this study. Duration time Δt_1 of its increase becomes shorter when oil supply becomes insufficient, and does not appear at all with running out of oil.

A time lag Δt_2 between a bottom of a valley in echo height variation curve and the sound axis of ultrasonic probe is also an effective evaluation index on insufficient oil supply. Δt_2 indicates the degree of differential of oil film formation condition between inflow region and outflow region. And Δt_2 has the potential which can detect the existence of slight oil at inflow region with high sensitivity than that of Δt_1. Hence, it is thought that Δt_2 decreases gradually when oil supply becomes insufficient, and becomes zero with running out of oil at a contact surface.

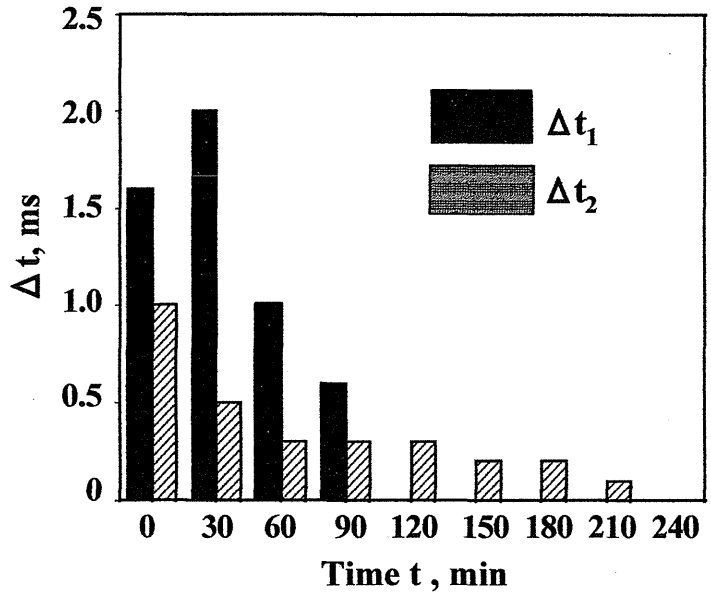

Figure 4 Variation of Δt_1 and Δt_2 measured by ultrasonic method

Figure 4 shows the variation of Δt_1 and Δt_2 measured by ultrasonic method at every 30 minutes, from start-up to 240 minutes. Δt_1 and Δt_2 are decreased gradually with passage of time, in particular Δt_2 which indicates the degree of difference of oil film formation condition between inflow region and outflow region shows continuous change for a long time. Therefore, it is considered that index Δt_2 is effective to evaluate the lubrication condition of ball bearing operated under a trace amount oil supply. And then, it can be estimated that effective oil film was existed at inlet region until 90 minutes, at least. In this way, these indexes are useful to evaluate the lubrication condition including oil insufficiency.

However, it is difficult to detect Δt_1 and Δt_2 in in-situ observation. More convenient method to evaluate the oil insufficiency is necessary for a lubrication diagnosis having hi-reliability. Upper figures in Figure 5 show the typical behavior of H_{T1} and H_{T2} from start-up to 1200min, and lower figures are the relationship between H_{T1} and H_{T2}. H_{T2} is used for the observation of oil insufficiency and the H_{T1} is for specifying the ball position and the sound axis of ultrasonic beam.

In those figures, notation '1' corresponds to the approaching process '1' shown in upper figure, notation '2'corresponds to the hump part of H_{T2}, '3' is the position where boll is on the sound axis, and minimum H_{T2} appeared at point '4' in start-up stage. The shape of those closed curves is varied with accumulation time. For instance, in case of sufficient oil supply condition, H_{T2} has a hump '2' after temporary decreasing, and minimum point '4' of H_{T2} appears in small H_{T1} region. However, such a hump of H_{T2} and minimum point corresponding to '4' do not appear, after passage of 240 minutes. Those closed curves are constantly repeated with passage of the ball if supply conditions of lubricant are the same. Then relationship between H_{T1} and H_{T2} shown by closed curve seems to be a useful index for in-situ observation of the oil supply condition.

However, it is not easy to make sure of a feature of a closed curve corresponding to lubrication condition instantly. Observation of the variation of closed curve area seems to be a useful index for the evaluation of the oil insufficiency rather than making sure of a feature of closed curve, since the area of closed curve decreases with the accumulation time as shown in Figure 5.

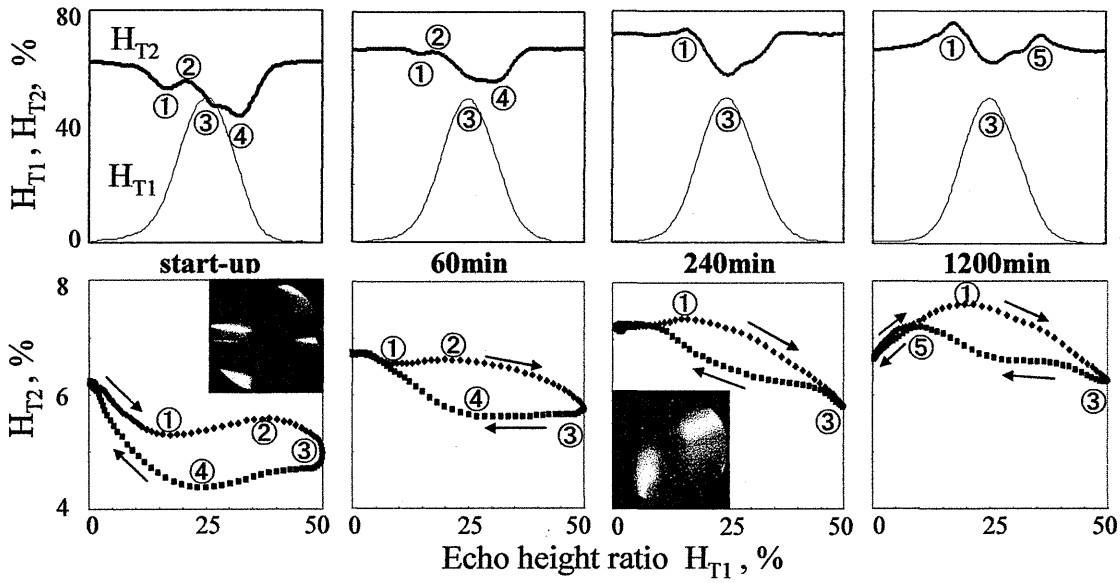

Figure 5 Behaviors of H_{T1}, H_{T2}, and relations between them

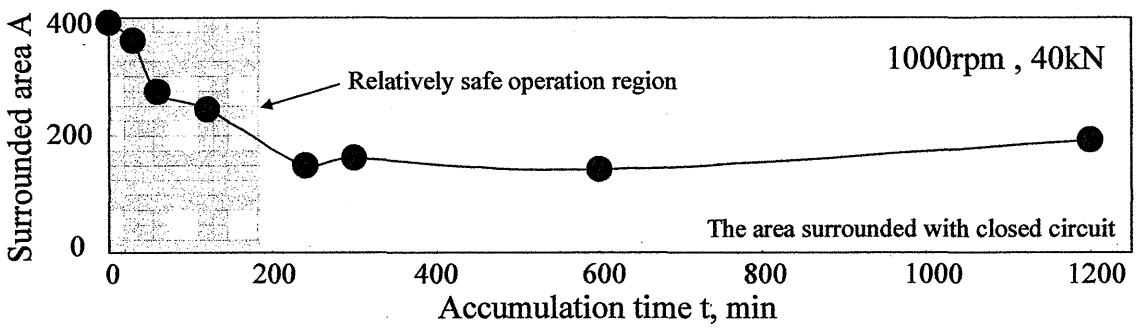

(a) Variation of surrounded area

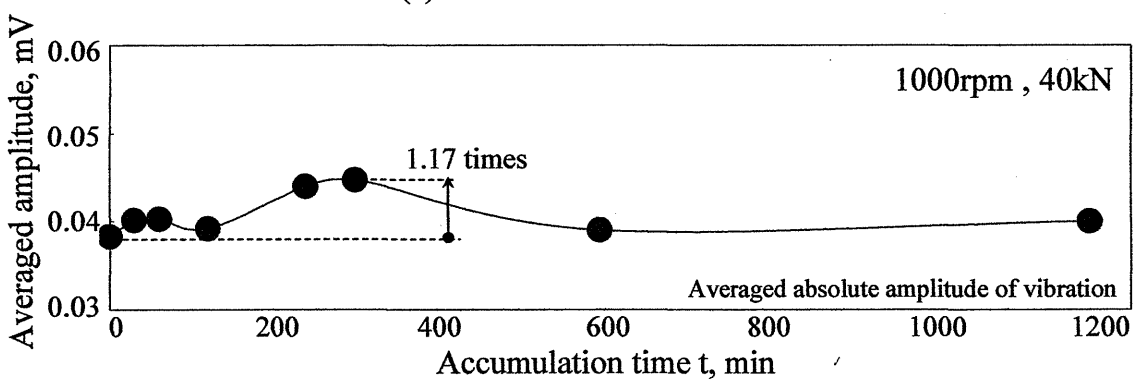

(b) Variation of averaged amplitude of vibration

Figure 6 Variations of surrounded area and average amplitude of vibration

Figure 6 shows the tendency of variation on the area of closed curve. The surrounded area in early stage of operation, from start-up to 240 minutes, is continuously decreased as supply of oil becomes insufficient. However, its area is kept almost constant after passage of 240 minutes because of running out of oil from the contact surface. So it is estimated from some indexes above that effective oil film was supplied until 90 min, in this case at least. In case of vibration shown in Figure 6, the remarkable variation of behavior such as closed curve area cannot be observed even though the vibration is slightly increased, 1.17 times, temporarily near 300 minutes.

4. Conclusions

The potential that is able to evaluate the lubrication condition of ball bearing operating under insufficient oil supply condition was clarified by the observation of behavior of ultrasonic echo height ratio H_{T2} reflected from the interface of ball and outer ring.

1) Oil supply condition at inlet side is shown by Δ_{t1}, and it approaches to zero as supply of oil becomes insufficient.
2) Differential of oil film formation condition between inlet region and outlet region is evaluated by Δ_{t2}, and it decreases in case of insufficient oil supply condition.
3) The area of closed curve formed by the relationship between H_{T1} and H_{T2} decreases with passage of time in early stage of operation. However, it is kept with almost constant value in case of insufficient oil supply condition.

References

[1] T. Yoshioka, S. Shimizu, H. Mano, A. Korenaga, H. Inaba and T. Wakabayashi: Journal of Japanese Society of Tribologists 51-8 (2006) pp. 607-614.
[2] T. Yoshioka and S. Shimizu: Journal of Japanese Society of Tribologists 55-11 (2010) pp. 819-826.
[3] A. Takeuchi: Key Engineering Materials 270(2004) pp. 252-257.
[4] A. Takeuchi, S. Terada and S. Toda: 3rd Asia International Conference on Tribology Kanazawa (2006) pp. 713-714.
[5] A. Takeuchi: Journal of Japanese Society of Tribologists 51-2 (2003) pp. 422-427.
[6] J. Zhang, B. W. Drinkwater and R. S. Dwyer-Joyce: ASME J. Tribol. 128 (2006) pp. 612-618.
[7] R. S. Dwyer-Joyce, B. W. Drinkwater, C. J. Donohoe: Proceedings of the Royal Society London A (2003) pp. 957-976.
[8] A. Takeuchi, S. Terada and S. Toda: International Conference on Advanced Technology in Experimental Mechanics (2007) pp. 42.

STUDY ON SURFACE QUALITY MEASUREMENT OF FLEXIBLE MATERIALS BY AIR JET

Osamu YOKOTA
Department of Mechanical Engineering, College of Engineering Nihon University. 1 Nakakawahara Tokusada Tamura-machi,Koriyama-shi,Fukushima,963-8642, Japan
E-mail:yokota@mech.ce.nihon-u.ac.jp

Kotaro YATABE
Doctor's Course, Mechanical Engineering, Graduate School of Engineering Nihon University. 1 Nakakawahara Tokusada Tamura-machi,Koriyama-shi,Fukushima,963-8642, Japan
E-mail:goblin@mua.biglobe.ne.jp

Mitsuo NAGAO
Department of Mechanical Engineering, College of Engineering Nihon University. 1 Nakakawahara Tokusada Tamura-machi,Koriyama-shi,Fukushima,963-8642, Japan
E-mail:nagao@mech.ce.nihon-u.ac.jp

Akitoshi TAKEUCHI
School of System Engineering,Kochi University of Technology
Tosayamada, Kochi 782-8502 Japan
E-mail:takeuchi.akitoshi@kochi-tech.ac.jp

Abstract: Measuring method for the softness and the viscoelasticity property has not yet been established. The test method which could measure the surface texture of soft objects for processed food and perishable foodstuff is established and the development of the functional equipment is desired. In this study, the dents were made to arise using air jet on the surface of soft object. The shape of the dents is measured in the two-dimensional laser beam. The measuring method of the softness was proposed by the measurement of diameter and depth of the dents which measured soft object. And the method for examining the viscoelasticity property by time course of the dents depth was proposed. The functional testing equipment based on them was manufactured and the soft object was measured. As a result, creep and creep recovery for the depth of the dents were clearly also obtained. Therefore, the measurement of soft object was possible for this measuring method, and it was possible to confirm the performance and the advantage.

Keywords: softness, creep, creep recovery, viscoelasticity, nozzle, laser-aided diagnostics, surface shape measurement

1. Introduction

To the best of our knowledge, there have been few reports on test methods for the viscoelastic properties of soft objects using an air jet instead of plungers for loading and unloading. We propose a method of evaluating their viscoelastic properties, such as soft processed foods and industrial products, using an air jet with newly developed test equipment.

In this method, loading and unloading can be performed using an air jet in a very short time, loading time can be arbitrarily set, and the shape of the dents formed on the surface of soft objects can be instantaneously measured using light from a semiconductor laser. In this study, using the developed equipment, we measured the shape of the dents formed on soft samples, measured the depth of the dents for various loading times, types of soft sample, and pressures, and evaluated the viscoelastic properties of the soft samples with respect to elastic compliance and equivalent dent depth.

2. Creep and Creep Recovery Compliances

Figures 1(a) and 1(b) show the creep and creep recovery curves and the four-element model used to obtain the curves, respectively. Figure 1(a) shows the curve of the creep compliance $J_{(t)}$ when a load is applied at t=0 and that of the creep recovery compliance $J_{r(t)}$ when the load is removed at $t=t_r$. In the creep phenomenon, the depth of a dent, $h_{(t)}$, increases with time, t, under a constant load F. In the linear viscoelastic creep phenomenon, in which $h_{(t)}$ is proportional to F, $h_{(t)}$ also increases with t under a constant load F. In this case, eq. (1) holds.

$$h_{(t)} = F \cdot J_{(t)} \quad , \quad \therefore \quad J_{(t)} = h_{(t)} / F \tag{1}$$

$J_{(t)}$ in eq. (2) can be divided into three terms as follows.

$$J_{(t)} = J_g + (J_e - J_g) \cdot \Psi_{(t)} + t/\eta \tag{2}$$

Here, J_g is the instantaneous compliance, J_e is the steady-state compliance at $t=\infty$, η is the viscosity coefficient, and $\Psi(t)$ is the creep function, which increases from $\Psi(0)=0$ to $\Psi(\infty)=1$.

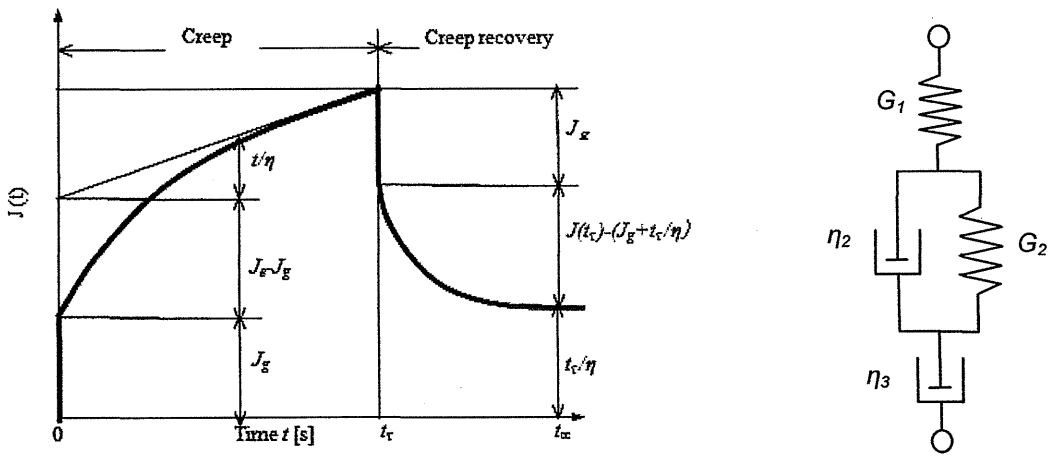

(a) Creep and creep recovery. (b) Four elements equivalent model.

Fig.1 Viscoelasticity property obtained creep and creep recovery.

3. Noncontact Measurement Method for Surface Texture

3.1 Measurement principle

Unlike conventional methods that use plungers for the loading of soft samples, the proposed measurement method uses an air jet with newly developed functional test equipment that can measure the softness and viscoelastic properties of foods and parts of living bodies. As shown in Fig. 2, air is ejected from a nozzle onto the surface of a soft sample. The surface of the soft sample does not deform when exposed to a weak air jet or when the distance between the nozzle and the sample is relatively long; however, it forms a dent when exposed to a strong air jet. Thus, the dimensions of dents are considered to greatly depend on the strength of the air jet. Therefore, the softness and viscoelastic properties of soft samples can

be determined by measuring the diameter and depth of dents for different strengths of the air jet and their changes with time. In the measurement of changes in the properties of viscoelastic samples with time, the developed test equipment has the following advantages: (1) The load to be applied to or removed from viscoelastic samples and its loading time can be arbitrarily set. (2) The loading process from the start of pressurization to the realization of the desired load and the unloading process from the end of pressurization to the realization of another desired load are almost instantaneous. (3) The state of deformation and the recovery of viscoelastic samples can be measured under conditions similar to those for loading or unloading using the air jet. (4) The damage and contamination of soft samples can be avoided owing to the noncontact nature of the method using compressed air.

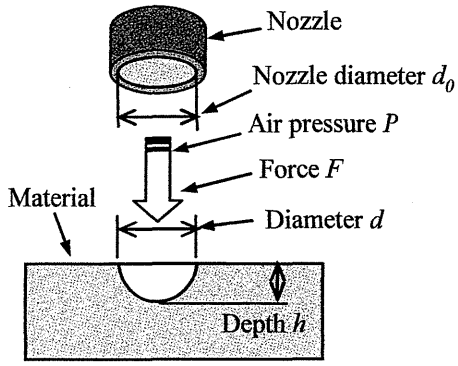

Fig.2 Measurement principle of surface texture

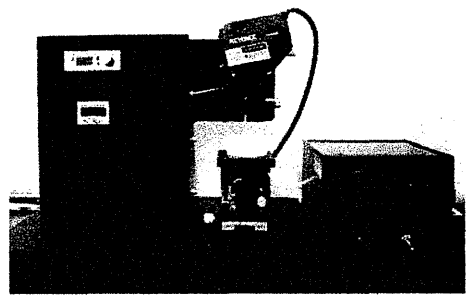

Fig.3 Summary of measuring equipment.

3.2 Noncontact-type test equipment using air jet

Figure 3 shows the noncontact-type functional test equipment, which comprises a compressor, an air tank for temporarily storing air, and a measurement unit. In the shape detection device, the depth and diameter of dents can be measured by irradiating visible light from a semiconductor laser with a large diameter onto a dent and collecting the reflected light using a two-dimensional charge-coupled device (CCD). The minimum measurable depth and dent diameter are 0.2 and 2.0 mm, respectively. A stable air jet was obtained when the nozzle diameter and ejection distance were 1.0 and 5.0 mm, respectively. The pressure explained in the experimental results section represents the pressure at the nozzle with the above dimensions, and the load was calculated from this pressure. The diameter and thickness of the

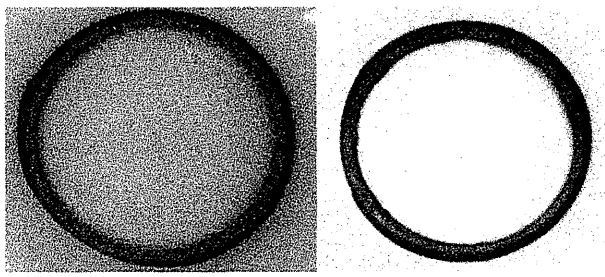

(a) Skin gel (b) Slime

Fig.4 Flexible materials for the experiment.

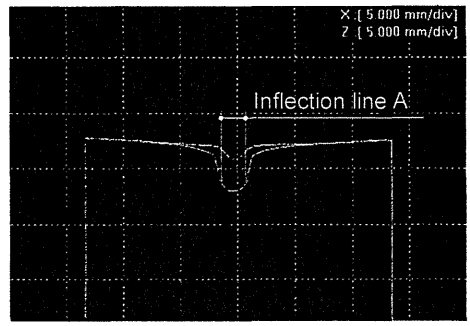

Fig.5 Cross section 2D shape which changed by the nozzle pressure.

soft samples used in this study were set to 50 and 20 mm, respectively, so as not to affect the measurement of the shape of dents. The samples used were human skin gel, slime, flan (or crème caramel), *kinu-dofu* (silken tofu) and *momen-dofu* (firm tofu).

4. Experimental Results

4.1 Viscoelastic properties for different loading times

Figure 5 shows the shape of the dent formed when the air jet was ejected onto the surface of the slime sample, obtained using the shape detection device. Figure 6 shows the creep and creep recovery curves for creep times of 5, 10, 15, and 20 s with the depth of the dent as the ordinate. Nonlinear delayed elastic deformation and viscous flow can be observed in the creep curves. The ratio of permanent deformation to elastic deformation decreased with increasing loading time. Therefore, it is considered that the elasticity of soft samples is related to the ratio of permanent deformation to elastic deformation caused by loading and that the elasticity of soft samples increases with decreasing loading time.

4.2 Viscoelastic properties of various soft samples

Measuring creep and creep recovery is an effective means of evaluating the depth of a dent formed on the surface of a soft sample when the surface is pressed or rubbed and how it recovers. Figure 7 shows the creep and creep recovery curves of samples of industrial materials (slime(green line) and human skin gel(purple line)) and processed food (flan(red line), silken tofu(light green line), and firm tofu(light blue line)) with the depth of the dent as the ordinate. In this experiment, the inner diameter of the nozzle was 1.0 mm, the ejection pressure was 20 kPa, the ejection time was 20 s, and the measurement time was 60 s. The depth of the dent up to a loading time of 7 s was greatest for the flan, indicating its greatest softness among all the samples. This was followed by slime, silken tofu, human skin gel, then firm tofu. After the loading time of 7 s, the depth of the dent on the slime exceeded that on the flan. This is considered to be because the instantaneous elastic deformation was dominant and the delayed elastic deformation and viscous flow were less dominant for the flan, whereas the viscous flow was dominant and the instantaneous and delayed elastic deformations were less dominant for the slime.

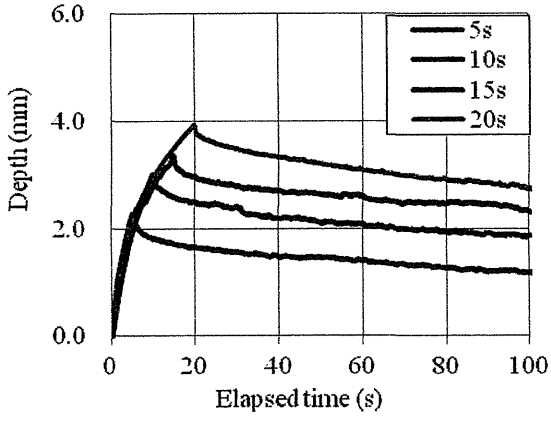

Fig.6 Variation of dents depth for creep time.

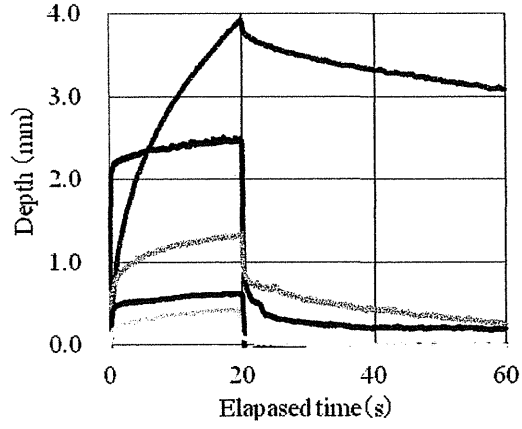

Fig.7 Elapsed time of dents depth which appeared on soft objects.

During the creep recovery for 40 s after the ejection had finished, the depth of the dent decreased most slowly with time for the slime. The depth of the dent was largest for the slime, which was followed by silken tofu, flan, then firm tofu. For the slime, instantaneous elastic

deformation hardly occurred and delayed elastic deformation was dominant. For the flan and silken tofu, three behaviors, i.e., instantaneous elastic deformation, delayed elastic deformation, and permanent deformation, were observed. For the human skin gel and firm tofu, the instantaneous elastic deformation was dominant during the creep recovery. From the above, the depth of the dent depends on the type of sample even under the same loading conditions, and therefore, soft samples can be compared and identified from differences in the depth of the dent; for example, slime is highly viscous, human skin gel is highly elastic, and tofu is viscoelastic.

4.3 Viscoelastic properties for various pressures of air jet

Figure 8 shows the changes in the depth of the dent with time when the human skin gel, slime, and silken tofu were exposed to an air jet. Five different pressures were applied and the inner diameter of the nozzle was 0.5 mm. To obtain the results for the human skin gel [Fig. 8(a)], ejection time was set to 30 s and pressure was changed in increments of 5 kPa between 40 and 60 kPa. Higher pressures were used for this sample than for the other samples because of the high elasticity of human skin gel. The depth of the dent was small at low pressures and large at high pressures. The dent was formed immediately after the start of loading and its depth sharply decreased immediately upon unloading, after which the human skin gel completely recovered within 5 s. This is because the rate of increase in dent depth was high when a load was suddenly applied, however, the viscosity was low and the creep recovery time was short when the loading time was short. Therefore, stress was considered to decrease in this time range. To obtain the results for the slime [Fig. 8(b)], which is a very soft material, ejection time was set to as short as 5 s and pressure was changed in increments of 5 kPa between 20 and 40 kPa. Comparatively low pressures were adopted to avoid breaking the surface of the slime with the air jet, which may disturb the measurement. It was found that the depth of the dent on the slime changed with time more slowly than that on the human skin gel at each pressure, showing that the viscous behavior was dominant with little elastic behavior. Although the depth of the dent exponentially decreased after unloading, the slime did not completely recover under any pressure even after a measurement time of 100 s, indicating its viscous behavior. The creep behavior of the silken tofu shown in Fig. 8(c) was intermediate between those of the human skin gel and slime. Elastic deformation was observed immediately after the start of loading, followed by viscoelastic behavior. Elastic deformation was also observed immediately after unloading, followed by a slow viscous recovery and plastic flow after a measurement time of 100 s. Waves with a short wavelength and a small amplitude were observed on each curve. This is considered to be because the final state of the tofu is affected by the generation of pores and the amounts of moisture, dietary fibers, and coagulants, and is nonuniform. For the silken tofu, ejection time was set to 20 s and pressure was changed in increments of 5 kPa between 20 and 40 kPa.

5. Discussion

5.1 Compliance in creep and creep recovery

The air jet ejected from the end of the nozzle causes soft samples to deform; the shape and dimensions of a dent formed on the sample surface depend on the distance from the end of the nozzle to the sample surface, i.e., ejection distance, even though nozzle pressure is constant. The load applied to the surface of the soft samples at each nozzle pressure when ejection distance was fixed at 5 mm was measured using a load meter in advance and used in the experiment. We measured the temporal changes in compliance, which is obtained by dividing the depth of the dent by the load. Compliance is given in mm/N, which is the inverse of spring constant, and represents the depth of the dent formed under a force of 1 N, i.e., the softness of a sample. Figure 9 shows the changes in compliance with time for the human skin

gel, slime, and silken tofu samples used to obtain the results in Fig. 8. For the human skin gel [Fig. 9(a)] and slime [Fig. 9(b)], the creep and creep recovery compliances at all pressures lie on almost exactly the same curve. Therefore, the effect of loading on the measured viscoelastic properties in the examined loading range is negligible for the human skin gel and slime. For the silken tofu [Fig. 9(c)], however, the creep and creep recovery compliance curves are different at different pressures. To explain this, it is assumed that the manufacturing method and standards for industrial products such as human skin gel and slime are uniform, meaning that they exhibit the predetermined mechanical properties and thus give similar results for hardness and tensile strength. In contrast, processed foods such as tofu and *kamaboko* (a Japanese processed seafood product) have nonuniform properties such as elasticity, hardness, and pore density. This may explain the result in Fig. 9(c).

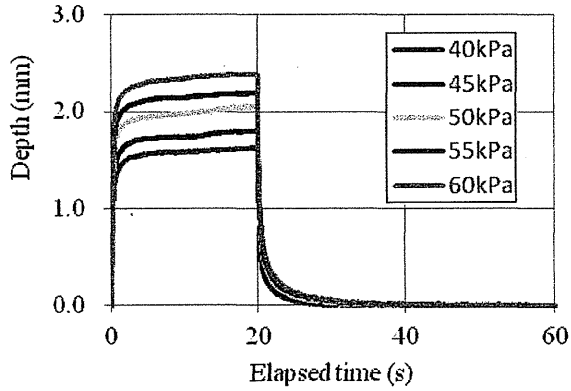

(a) Skin gel

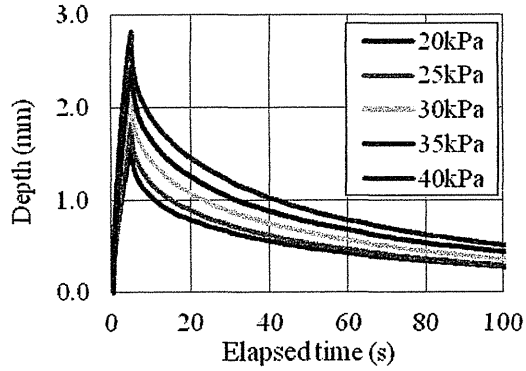

(b) Slime

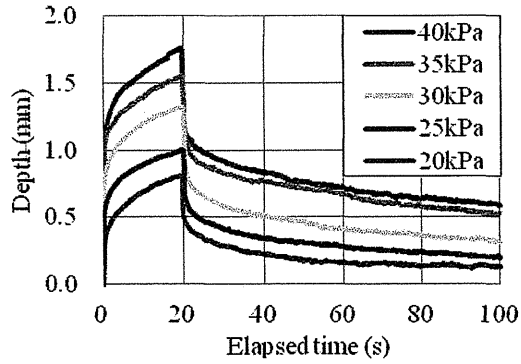

(c) Silk tofu

Fig.8 Elapsed time of dents depth on soft objects for pressure.

5.2 Equivalent dent depth in creep and creep recovery

In Fig. 8, the ratio of dent depth at an arbitrary time to the maximum depth at the end of creep or immediately before creep recovery is defined as the equivalent dent depth, which is a dimensionless value. Figure 10 shows the changes in equivalent dent depth with time for the human skin gel, slime, and silken tofu used to obtain the results in Fig. 8. For the human skin gel [Fig. 10(a)] and slime [Fig. 10(b)], the equivalent dent depths during creep and creep recovery at all the pressures lie on almost exactly the same curve, similar to the case of compliance shown in Fig. 9. For the silken tofu [Fig. 10(c)], however, the curves of equivalent dent depth do not fit on a single curve, similar to the compliance curves shown in Fig. 9(c). From the above, compliance or equivalent dent depth can be used to describe creep and creep recovery behaviors.

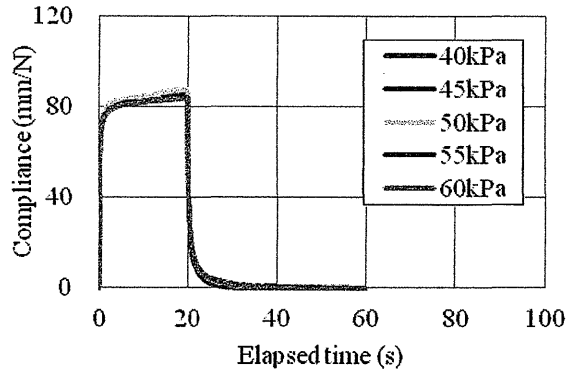

(a) Skin gel

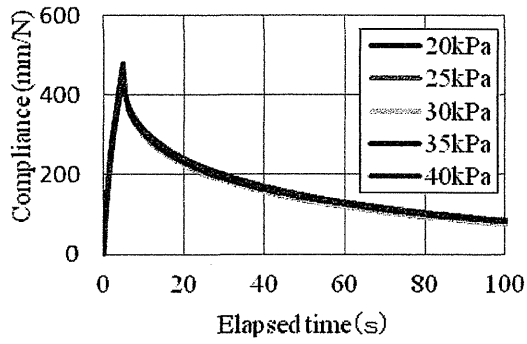

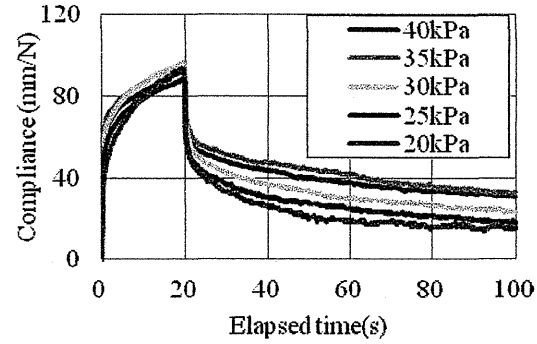

(b) Slime (c) Silk tofu

Fig.9 Elapsed time and compliance for pressure.

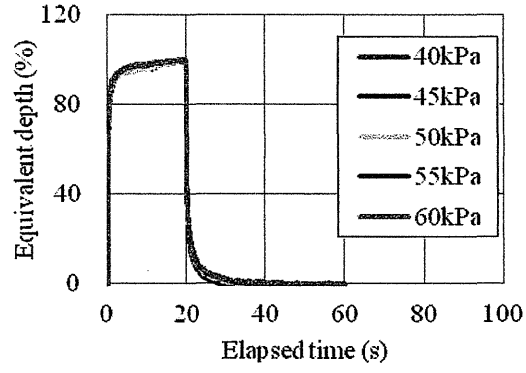

(a) Skin gel

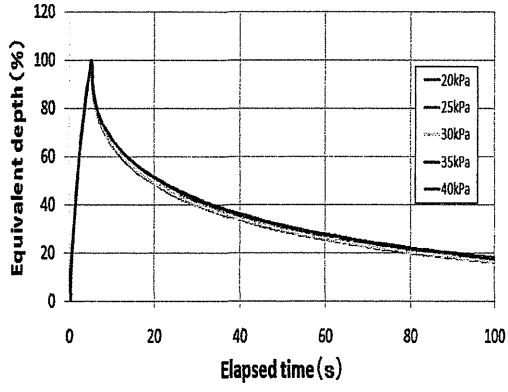

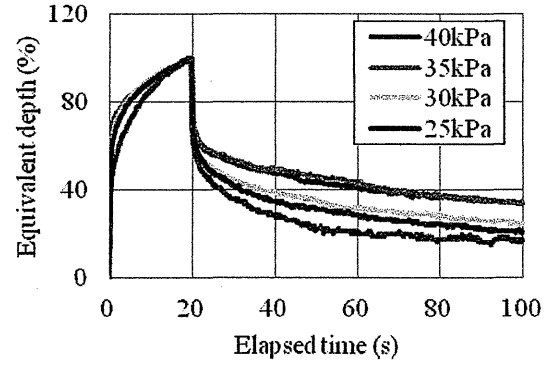

(b) Slime (c) Silk tofu

Fig.10 Elapsed time and equivalent depth for pressure.

6. Conclusions

In this study, using the developed equipment, we measured the shape of the dents formed on soft samples, measured the depth of the dents for various loading times, types of soft sample, and pressures, and evaluated the viscoelastic properties of the soft samples with respect to elastic compliance and equivalent dent depth. The results are reported below.

(1) The creep and creep recovery curves of dent depths were shown for creep times of 5, 10, 15, and 20 seconds.
(2) These curves of samples of industrial materials and processed food were measured the depth of the dent as the ordinate.
(3) The creep and creep recovery compliances at all pressures lie on almost exactly the same curve.
(4) The equivalent dent depths during creep and creep recovery at all the pressures lie on almost exactly the same curve, similar to the case of compliance.

References

[1] Brandt M.A., Skinner E.Z. and Coleman J.A. :Texture profile method, *J.Food Sci.*, 28, 404 (1963).
[2] Szczesniak A.S., *Effect of storage on texture in food storage stability*,Eds.,Taub I.A. and Singh R.P.(CRC Press), 191 (1997).
[3] Seiji YOSHIKAWA and Motoh OKABE,Texture Profile Pattern of Foods by Profile Terms and Texturometer ,*Rept. Natl. Food Res*, Inst.,No. 33, 123-129 (1978).
[4] Tsukasa NISHIMURA, Jyunzo SUZUKI, Takehiko FUKUDA : Application of table-top universal tester to food texture, *Shimadzu review* 65(1・2)55-59、2008.
[5] JIS Z 2244:2009 Vickers hardness test -- Test method
[6] JIS Z 2243:2008 Brinell hardness test -- Test method
[7] ISO 7619–1:2004, *Rubber, vulcanized or thermoplastic -- Determination of indentation hardness -- Part 1:Durometer method (Shore hardness)* (2004).
[8] TANAKA M., Development of a Haptic Sensor for Monitoring skin conditions, *J. of JAPAN SOCIETY FOR DESIGN ENGINEERING*. 39-3(2004), pp. 134 -137.
[9] Roderic S.Lakes, *VISCOELASTIC SOLIDS* (1998), p.4, CRC Press.
[10] NAGAO M., SAKAI Y. and YOKOTA O., Development of Non-contact Softness Tester, *J. of JAPAN SOCIETY FOR DESIGN ENGINEERING*. 41-5(2006),pp.267-272.
[11] Yokota O., Softness Measuring Method and Softness Measuring Equipment., *Patent*, JP, P4247474(2009).
[12] Grolman B.: A new tonometer system, *American J. Optom Arch Amer Acad Optom,* 49 (1972), pp.646.
[13] UCHIDA K., Concerning Tonometry (The Development and the Newest Model of Noncontact Tonometry), *J. of JAPAN SOCIETY FOR DESIGN ENGINEERING*, 39-3(2004), 138-142.

DEVELOPMENT OF A MUSCLE HARDNESS TESTER AND ITS MEASUREMENT CASES

Mitsuo NAGAO
Department of Mechanical Engineering, College of Engineering, Nihon University. 1 Nakakawahara Tokusada Tamura-machi, Koriyama-shi, Fukushima, 963-8642, Japan
E-mail: nagao@mech.ce.nihon-u.ac.jp

Shin-ichi KONNO
Department of Orthopedic Surgery, Fukushima Medical University. 1 Hikariga-oka, Fukushima-shi, Fukushima, 960-1295, Japan

Tokuo ENDO
Endo-Osteopathic Clinic, Director. 3-2 Kajimen Motomiya Motomiya-shi, Fukushima, 969-1129, Japan

Kotaro YATABE
Doctor's Course, Mechanical Engineering, Graduate School of Engineering, Nihon University. 1 Nakakawahara Tokusada Tamura-machi, Koriyama-shi, Fukushima, 963-8642, Japan

Osamu YOKOTA
Department of Mechanical Engineering, College of Engineering, Nihon University. 1 Nakakawahara Tokusada Tamura-machi, Koriyama-shi, Fukushima, 963-8642, Japan

Abstract: As the background of our study, we requested that practitioners use muscle hardness testers to conduct a digital assessment of the muscle hardness layers that they can feel by palpation. We developed muscle hardness testers to assess muscle hardness digitally from the reaction force and the depth in pushing a finger-shaped indenter, thereby simulating palpation. As described in this paper, we confirmed the effectiveness of digital assessment using foam rubber consisting of an upper layer and a lower layer, respectively simulating the cortical and muscle layers of a human body. Additionally, we digitally assessed the change of hardness of the trapezius muscle by changing the position of the upper extremity. Next, we were able to measure the change of hardness before and after treatment for subjects with shoulder stiffness. Results show that the proposed tester contributes to digital assessment of muscle hardness and palpation hardness.

Keywords: trapezius muscle, palpation, muscle hardness tester, finger-shaped, foam rubber, shoulder stiffness

1. Introduction

This study was undertaken to develop a muscle hardness tester to assess muscle hardness digitally when a finger-shape indenter, simulating palpation, is pushed into a muscle [1]. Commercially available testers and those described in the literature [2-10] present benefits and shortcomings, but the practitioners who actually conduct medical treatment have never actually evaluated such testers. Moreover, because subjects have idiosyncratic differences in body shape, constitution, and object sites, existing testers are not adjusted to these conditions. Additionally, such testers offer little quantifiable operability and reliability. The proposed tester was designed to assess muscle hardness digitally, free of the influence of various conditions. The tester can recognize small differences of hardness, hardness of deep muscle layers, and the effects of treatment and follow-up care. This report describes the outline and digitalization mode of the proposed equipment and confirms its effectiveness and validity through the following experiments: first, the hardness of the lower layer of the double-layer foam rubber is assessed digitally; second, hardness is measured when the trapezius muscle is constricted; third, hardness is assessed digitally before and after treatment for shoulder stiffness. Hereinafter, we describe details of how we reached our conclusions.

2. Muscle hardness test equipment

2.1. Composition of the muscle hardness tester

Figure 1 shows the process of manual palpation (by fingers) of a muscle induration (a stiff muscle site). As Figure 2 show, this proposed device can simulate the movement of a finger pushing the induration. Figure 3 depicts the relation of the reaction force W and depth x, when the intender, representing a finger, is pushed into the skin. By holding the upper part of it by hand, the pushing is conducted at 9 mm of stroke for five seconds. The reaction force and the depth are obtained respectively from the load cell and the displacement. Then those data are sent to the PC for digital processing. With the PC, digital processing in Figure 3 and that described hereinafter are conducted. The results are shown on the display. Consequently, because the thickness of the upper layer and the middle layer shown in Figure 1 has individual differences and site differences, the experimenter must manipulate it by adjusting the pushing force of the finger searching for the hardness. The pushing force W_0 is equivalent to the load adjustment shown in the upper part of Figure 2.

The main specifications are described in the following: The indenter diameter is 8 [mm]. Its material is POM; at the tip is a ball with 4 [mm] radius. The keep plate diameter is 40 [mm]. Its material is also POM. Pushing is conducted at a stroke of 9 [mm] for 5 [s]. The range of pushing force is W_0=2– 40 [N]. The range of displacement is x=0–15 [mm].

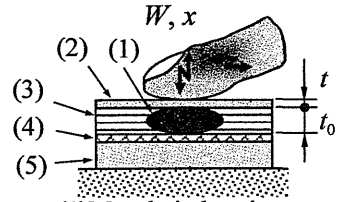

(1)Muscle induration
(2)Surface (epidermis, fat)
(3)Muscle layer
(4)Muscle lower layer
(5)Lower layer (Skeleton)

Figure 1 Palpation of the muscle induration by the finger

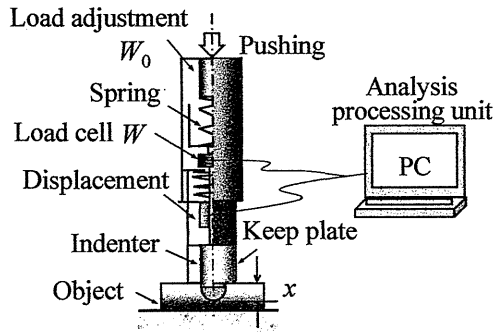

Figure 2 Outline of muscle hardness test equipment

The total height is 155 [mm] and the mass is 650 [g]. The body casing is made from stainless steel. It is possible to change the indenter and the keep plate depending of the figure of an object site. Additionally, W_0 is the value when the tester on the steel plate 10 [mm] thickness is pushed into at pushing stroke of 9 [mm].

2.2. Methods of quantification

According to the range of x shown in Figure 3, the initial stage, the metaphase, and the telophase of pushing represent the hardness of the cortical layer including the fat layer, the fat layer to muscle layer, and the object site, respectively, by the correlation of W-x. The hardness is obtained from the pushing reaction force W [N], the pushing depth x [mm], the elastic constant $\kappa=W/x$ [N/cm], and differential elastic modulus $\tan\theta=\Delta W/\Delta x$ [deg] [1]. Although the representation with W or x might resemble the methods used by existing mechanical hardness testers [2-4], this method is useful when the difference of hardness of objects is large. When it is difficult to judge the difference using this method, κ is added for judgment. Even so, when it is difficult, one must conduct multiple judgments adding the gradient at the end of pushing $\tan\theta$. Furthermore, because it is possible to adjust the pushing force depending on the conditions such as the cortical layer thickness or the object site hardness as shown in Figure 2, it is also possible to make measurements that approximate the hardness felt by palpation.

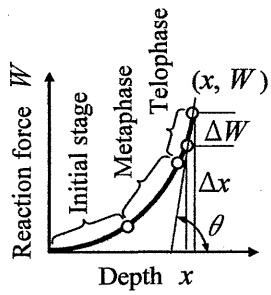

Figure 3 Digitization of the muscle hardness (W-x curve)

Table 1 Composition of the samples of two layers

Composition	Type of the samples *				Pushing force
Symbol	AA	AB	AC	AD	W_0 [N]
Upper layer	A sponge, t=5 [mm]				4, 8, 12, 20, 24, 28, 32, 36
Lower layer t_0=10 [mm]	A	B	C	D	
Durometer Type E [hardness]	E21 ±2/5	E23 ±2/5	E38 ±2/5	E47 ±2/5	

* Foam rubber dimensions; $t\times W\times \ell=t\times 50\times 100$ [mm]

3. Experiments and results

3.1. Pushing force assessing the lower layer hardness

We confirmed the effectiveness of our proposed digitalization method by the pushing force, which can assess the change of the lower layer hardness, by maintaining the upper layer thickness constant for two layers consisting of the upper layer of the surface layer (2) and the lower layer of the muscle layer (3) presented in Figure 1. Conditions of the two layers are shown in Table 1. The upper layer is made of foam rubber A ($t\times W\times \ell=5\times 100\times 50$ [mm], E21). The lower layers with different hardness are made of four kinds of foam rubber A–D ($t_0\times W\times \ell=10\times 100\times 50$ [mm]). The combinations of composition are symbolized by AA, AB, AC and AD. The foam rubber hardness is represented by the values of Durometer Type E. The pushing forces are divided into eight levels of 4 [N] to 36 [N].

Results of the experiments show that the correlation between pushing reaction force W and pushing depth x are as portrayed in Figure 4(a). The elastic constant κ and the differential elastic modulus θ are in Figure 4(b). All results are mean values obtained from 10 pushing repetitions. The "4 Mono" shown in Figure 4 means the values in directly pushing it into the samples A–D with pushing force of 4 [N]. To clarify the differences before and after the sample, the symbols are connected with a line. The amount of W_0 by which the differences between AA and AB, between AB and AC, and AC and AD can be judged, was obtained

using t-tests. Assuming that the two samples are homoscedastic, the conditions were obtained with two-sided t boundary values, significance level of p=0.0001, and degrees of freedom of φ=18. The result was $t(\varphi, p)=t(18, 0.0001)=4.97$. In terms of W_0, with the test statistic of $t_0>t$, x, W and κ had $W_0>20$ [N] and θ had $W_0>8$ [N]. Consequently, if each pushing force equivalent to the thickness of the upper layer is appropriate, then it is possible to assess the different hardness of the lower layers digitally. It can be applied directly to the thickness of (1) and (2) in Figure 1. In the digitalization of θ, even if W_0 is smaller than the others, the differences can be discriminated as the advantage of this equipment.

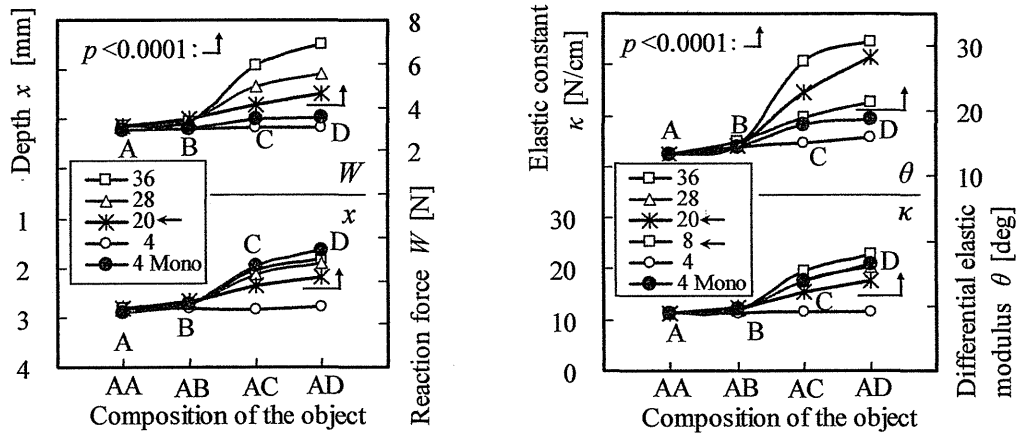

(a) Quantification by x and W (b) Quantification by κ and θ

Figure 4 Effect of pushing force to assess the lower layer hardness

3.2. Comparison between κ and θ by the upper layer thickness

We confirmed the effect of the upper layer thickness on the sensitive reference in digitalization of κ and θ when foam rubber A with thickness of t=1, 2, or 3 [mm] was put on the lower layer shown in Table 1. The results are shown in Figure 5. Indications "Mono" are values of A–D. In digitalization of elastic constant, as the upper layer becomes thicker, the difference between objects becomes indistinct. Therefore, with t=3 [mm], it becomes more difficult to determine it than with t=1 [mm]. On the other hand, in digitalization of θ, unlike in κ, without difference of an upper layer, we conducted an ANOVA (p<0.01, one-way analysis, level of factor 4, and repetition number of times 10) for every different composition of the objects (e.g., in the case of AA, four kinds of θ including single layer A, and layers with t=1, 2, and 3 [mm]). The discriminant standard is that shown below.

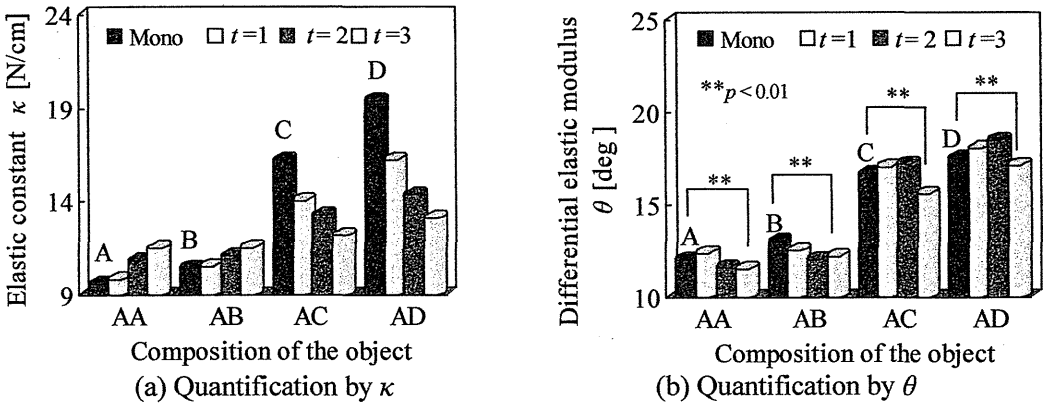

(a) Quantification by κ (b) Quantification by θ

Figure 5 Sensitivity comparison between κ and θ

$$F_0(\varphi_A, \varphi_E; 0.01) = F_0(3, 36; 0.01) = 4.38$$

The values F of the objects were the following: AA(1.69), AB(1.02), AC(2.64), AD(1.57). Consequently, because $F<F_0=4.38$ in all the objects, it turned out to be difficult to assess the change of the upper layer thickness digitally. In Figure 5, we described it as $**p<0.01$. In digitalization of θ, even if W_0 is small, as shown in Figure 4, its sensitivity is so higher than in κ as to show the difference of the lower layer hardness.

3.3. Contraction hardness of trapezius muscle by eversion of the arm

This experiment confirms the possibility of digitally assessing the hardness before and after a trapezius muscle contracts. The contents are shown in Table 2. Examinees were six university students with different body shape and features of physical constitution: they were designated as A1–A6 in order of increasing Body Mass Index (*BMI*) values. The hardness of contracting muscle was obtained from the posture in which the position of upper extremity was different at two sites. First, the muscle was not tense and soft when the upper extremity was put on the armrest. Second, the muscle contracts and becomes tight when the first position of the upper extremity turns outward by 90 deg. The site on which the intender is placed is midway between the seventh cervical spine and the acrominon, where the hardness can be felt by fingers.

Table 2 Features and measurement condition of six examinees: university students, age 21–22

Examinees No.	A1	A2	A3	A4	A5	A6
BMI value	19	21	21	22	24	24
Features of the body	Thinness type Thin muscle layer	Normal type Thick muscle layer	Normal type	Normal type Tennis player	Small fatness type	Small fatness type Thick muscle layer
Object position	Trapezius muscle of the right shoulder, the position which guesses the indenter is a midpoint of cervical spine C7 and acromial process.					
Contraction action of the arm	It sits in the armchair, and armrest position and 90-deg turning outward position.					
Measurement condition	Indentation set load W_0=9.8[N], keep plate diameter 40[mm], indentation setting hour 5[sec], the tip is a globe on the indenter diameter at 8[mm] and pushing frequency 5 [times].					
	BMI value [kg/m²]: Thinness type≦19, 19 < Normal type < 24, 24 ≦ Small fatness type < 28, 28≦Obesity type					

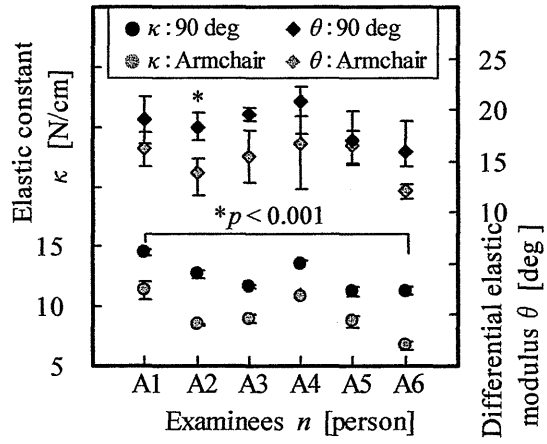

Figure 6 Comparison of muscle hardness by muscle contraction of trapezius muscle

In Figure 6, examinees A1–A6 are on the X axis; the hardness of armrest position and 90-deg turning outward position in terms of κ and θ are shown on the Y axis. Along with the mean value, the range of the maximum value and the minimum value is also shown. According to $\kappa=W/x$, the difference between conditions before and after muscle contraction is evident, so it is possible to assess the muscle hardness digitally. Although the experiment did not assess the thickness of fat layer and muscle layer digitally, to assume the correlation between *BMI* and the thickness of those layers, it is reasonable to expect that the value should be smaller. Examinee A4, a tennis player, has hard and thick neck and shoulder muscles, which is represented by the value. A1, who is thin, has a large value when his upper extremity was put on the armrest. To assume that his muscle is also proportionally thin, it should be because the value also represented the bone layer hardness as well as muscle layer or the pushing force was strong. On the other hand, even though the tendency in digitalization by θ is like that shown by κ, results show that the variation of values is greater than that by κ. That tendency might be attributed to the high sensitivity shown in Figure 5. Showing the effectiveness of our proposed digitalization, when the difference in, for example, A5 is evident by κ, but difficult to discriminate by θ, one can discriminate it with $\kappa= W/x$.

Next, using the t-test, we confirmed that the muscle hardness in turning outward position can be discriminated to be higher than that in armrest position. As the test conditions to find the values, two samples are assumed to be homoscedastic. The t boundary value is one-way. The significance standard is p=0.001. Degrees of freedom are φ= 8. In digitalization by κ and θ, $t(\varphi, 2p)= t(8, 0.001)$=4.50 was found. In digitalization by κ, the test statistic t_0 was $t_0>t$ in all examiners. Digitalization by θ it was so in only A2, which is shown as "*p<0.001" in Figure 6.

The experiment demonstrated the following. It is important to assess the hardness of each rather than the differences of hardness among individuals because human bodies have individual differences related to thickness and hardness of the object sites, as shown in Figure 1 and Table 2. Furthermore, as shown in Table 1 and Figure 4, because the thickness is a factor holding the key to the sensitivity of the hardness, for measurement with good sensitivity, it is necessary to imitate the movement of strong pushing when the object site is thick. When the thickness is slight, even small change can grasp if one lightly pushes the indenter as in palpation.

3.4. Muscle hardness around the operation of shoulder stiffness

The examinees were 21 male university students aged 21–4 (B1–B21), for whom we had conducted a survey in the form of a questionnaire. We obtained their consent for the experiment in advance. The object sites were the site of shoulder stiffness which we located by palpation and near which the indenter was pushed, with the same measurement conditions as those in Table 2. Before and after a practitioner gave an examinee a massage, we measured the hardness with our muscle hardness tester five times, with the mean considered as the measured value. The practitioner gave a massage by hand and used an ultrasonic therapy apparatus for about four minutes. For the amount of change before and after the treatment practice, we conducted a t-test, assuming that two samples should be homoscedastic. With a two-sided t-boundary value (p<0.05), we obtained $t(\varphi, p)=t(8, 0.05)$=2.31. The examinees were divided into three groups based on this test: a group of the examinees whose muscle softened (13 by κ and 9 by θ among 21), a group showing no difference (5 by κ and 11 by θ among 21), and a group of examinees whose muscle became harder (3 by κ and 1 by θ among 21). In Figure 7, with κ represented on the left vertical axis, the three groups are shown from right to left (represented by two bar charts). They are arranged in ascending order of muscle hardness. The horizontal axis represents the values of examinee numbers and their *BMI*.

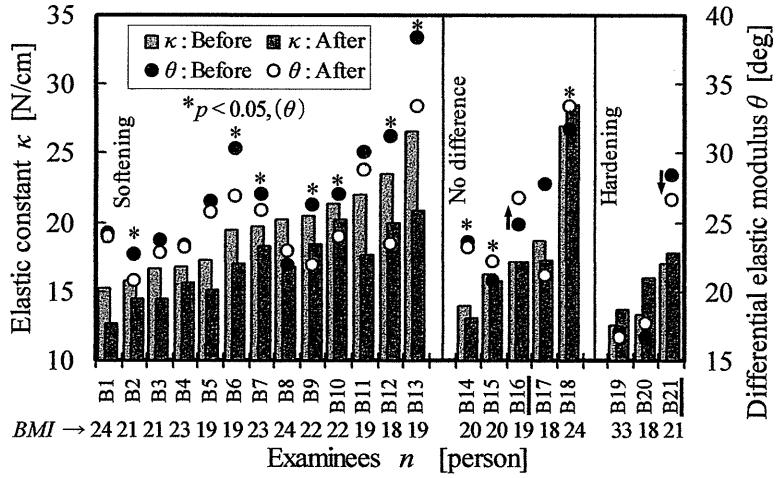

Figure 7 Muscle hardness of shoulder stiffness

On the other hand, with θ represented on the right vertical axis (by signs of circle), each θ of the examinees, divided into three groups by t-test, is marked by a reference mark [*] (*p<0.05).

They were divided into three groups because the practitioner explains that physical stimulus was given to a stiff muscle for which the tissues' blood circulation was facilitated, thereby softening it. Others showed no difference. Other muscles showed increasing inner pressure of the muscle, thereby hardening it. B16 (no difference by κ, hardening by θ ;↑) and B21 (hardening by κ, softening by θ ;↓) showed different judgment by κ and θ. With the boundary value of p<0.01, they have the same judgment by κ and θ. Therefore, it is possible to assess the muscle hardness digitally based on changes that occur during physical treatment for patients with complaints of shoulder stiffness. Results show the capability of digital assessment of the effects of practical treatment and palpation.

In Figure 8, the *BMI*, shown on the horizontal axis, is arranged in ascending order, different from Figure 7, and a regression line is added. The *BMI*-33 [kg/m^2] of B19 indicates the obesity-type according to Table 2. From both regression lines, the line after practice is located below because muscles of many examinees softened considerably. The gradient is on the downside, presenting the possibility that the surface layer thickness shown in Figure 1 is correlated with the *BMI*.

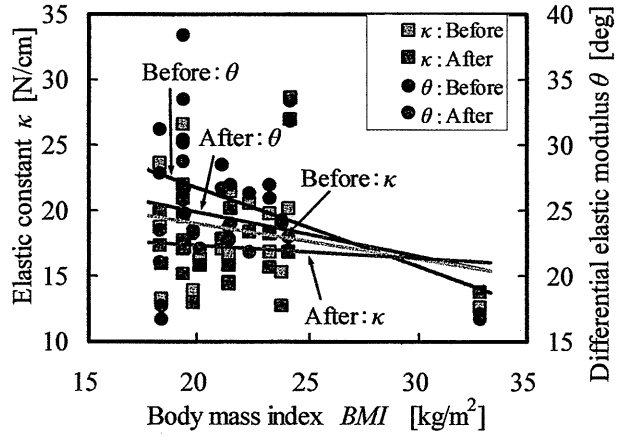

Figure 8 Correlation of muscle hardness and *BMI*

4. Conclusions

Proposing an outline of the muscle hardness tester that can imitate hardness assessments done by palpation and presenting a mode of to digital assessment, we were able to confirm their effectiveness and validity by conducting several experiments. The obtained results are summarized as follows:

(1) We proposed four methods to assess muscle hardness digitally. Using them singly or multiply, the tester presents high reliability. κ and θ are used in typical methods.
(2) Discriminating the lower layer hardness for different surface thickness is possible if the pushing force is appropriate to thickness.
(3) For a thin surface layer, such as a few millimeters, θ has less effect on the lower layer hardness than κ does, and is therefore validated. Furthermore, θ is more sensitive than κ.
(4) The muscle hardness before and after practical treatment for shoulder stiffness can be categorized into three groups: softening, no difference, or hardening. They are highly correlated to κ and θ, with some exceptions.
(5) In future studies, we will aim at improving the process for practical application by examining the possibilities of digitally assessing effects according to practices, substitution of palpation or self-palpation, and follow-up.

Acknowledgement

Part of this study is conducted with assistance provided by a Grant-in-Aid for Scientific Research C (No. 22560225). We express our gratitude for that support.

References

[1] Nihon Univ., *Hardness test method, hardness test equipment and hardness measuring device*, Patent No.2009-052912, JP, (2009).
[2] Imoto machinery Co. Ltd., *The muscle hardness tester*, Patent No.3951257, JP, (2007).
[3] S. Hiwatari, et. al., *The muscle hardness tester*, Patent No.4352022, JP, (2009).
[4] Ito Co., Ltd., *The muscular tissue hardness tester*, Patent No.4922056, JP, (2012).
[5] N. Motooka, et.al., *Development of New Instrument to Assess Visco-Elasticity of Skin and Muscle*, Technical Digest of the 15th Sensor Symp., pp.87-92, (1997).
[6] A. Takanashi, et. al., *Reliability of Measurement of Elastomer Samples by Soft Tissue Stiffness Meter*, Rigakuryoho Kagaku, 24(1), pp.31-34, (2009).
[7] H. Andersen, et. al., *Pressure Pain Sensitivity and Hardness Along Human Normal and Sensitized Muscle*, Somatosensory and Motor Research, 23(3), pp.97-109, (2006).
[8] Y. Arima, *Objectification of Hardness Information of Palpation*, The bulletin of Meiji University of Oriental Medicine, No.25, pp.25-49, (1997).
[9] Y. Tsuda, et. al., *An Examination for Measuring the Softness of Human Shoulders (1)*, J. Intl. Soc. Life Info. Sci., **23**(2), pp.332-334, (2005).
[10] F. Ito, et. al., *The Effects of Electric Field Therapeutic Device (Healthtron) on the Stiffness in the Neck and Shoulder Area*, J. Jpn. Soc. Balneol. Climatol. Phys. Med., **68**(2), pp.110-121, (2005).